

## CONCENTRATION OF TOROIDAL MAGNETIC FIELD IN THE SOLAR TACHOCLINE BY $\eta$ -QUENCHING

PETER A. GILMAN AND MATTHIAS REMPEL

High Altitude Observatory, National Center for Atmospheric Research\*, P.O. Box 3000, Boulder, Colorado 80307, USA  
*Draft version October 29, 2018*

### ABSTRACT

We show that if the turbulent magnetic diffusivity used in solar dynamos is assumed to be 'quenched' by increasing toroidal fields, much larger amplitude and more concentrated toroidal fields can be induced by differential rotation from an assumed poloidal field than if there is no quenching. This amplification and concentration mechanism is weakened and bounded by  $\mathbf{j} \times \mathbf{B}$  feedbacks on the differential rotation. Nevertheless, it is strong enough to contribute to the creation of  $\sim 100$  kG toroidal fields near the base of the convection zone, perhaps in conjunction with the 'exploding flux tube' process. Such high fields are necessary for sunspots to occur in low solar latitudes.

*Subject headings:* Sun: interior — rotation — magnetic field

### 1. INTRODUCTION

There are substantial theoretical reasons for concluding that sunspots and active regions arise when toroidal flux tubes in or near the solar tachocline erupt to the photosphere (Fan et al. 1994; Schüssler et al. 1994; Caligari et al. 1995, 1998). Given the Sun's rotation rate, for these eruptions to occur in low solar latitudes where spots are found requires that the tubes in the tachocline have field strength approaching 100 kG (Choudhuri & Gilman 1987). Such large fields are a potential problem for dynamo theory applied to the Sun, since they are locally 10 – 100 times the equipartition value when compared to the kinetic energy density of both convective turbulence and differential rotation at tachocline depths.

In all interface and flux transport dynamos applied to the sun, the strong toroidal fields achieved at tachocline depths come from the shearing by differential rotation there of a much weaker poloidal field. These toroidal fields are of much higher amplitude there than in the convection zone above because the magnetic diffusivity is assumed to be much smaller than in the much more turbulent convection zone. Since this shearing is also likely to lead to a back reaction on the local differential rotation, thereby extracting energy from it to amplify the magnetic field, the peak field achieved by induction depends critically on the rate energy can be resupplied to the differential rotation by the convection zone above. To be effective, this energy must be resupplied in a time quite short compared to a sunspot cycle. Since helioseismic inversions for differential rotation in the neighborhood of the tachocline do not show significant changes in the differential rotation within a solar cycle, whatever resupply is needed must be taking place. Indeed, the relative constancy of the observed differential rotation supports the validity of kinematic type dynamo models for the solar cycle, but sets constraints on the efficiency of the resupply mechanism and/or the toroidal field amplitudes produced by the shear. The resupply mechanism is not understood in detail, and any additional mechanism

that helps produce concentrated high amplitude toroidal fields potentially reduces the amount of resupply needed and may allow higher toroidal fields to be produced for the same feedback.

A promising mechanism for achieving super-equipartition field strengths that does not depend totally on differential rotation is that of rising flux tubes 'exploding' before they reach the photosphere (Moreno-Insertis et al. 1995; Rempel & Schüssler 2001). In this scenario, many explosions of tubes result in significant loss of mass from inside the tubes, so that the part of the toroidal field that remains in the tachocline becomes more concentrated. If this happens at the unseen beginning of a new sunspot cycle, then the concentration of flux can lead to sufficient field strength that subsequent tubes get to the photosphere before they explode, so they can emerge as active regions.

Here we propose another, perhaps complementary, mechanism for concentrating toroidal magnetic flux, involving the effect of turbulence, and therefore turbulent diffusivity, being partially or even largely suppressed where the toroidal fields are strong. The effects of this " $\eta$ -quenching" have been considered more broadly in dynamo theory previously by, for example, Rüdiger et al. (1994) and Tobias (1996), but without our emphasis on locally strong amplification of toroidal fields. Rüdiger & Kitchatinov (2000) included the effect of " $\eta$ -quenching" together with quenching of turbulent heat conductivity in a model for the decay of sunspots. We use a formulation quite similar to that commonly used in dynamo models for " $\alpha$ -quenching" (Dikpati & Charbonneau 1999) (We make no attempt to evaluate the relative merits of various formulations of the  $\eta$ -quenching with guidance from MHD turbulence theory, such as is done in Vainshtein & Cattaneo (1992)). Our results below show that this  $\eta$ -quenching can be an extremely powerful mechanism for concentration when one is solving only the induction equation, but can be damped considerably when feedbacks on the differential rotation are taken into account. Thus this mechanism is subject to similar energetic limitations as when no  $\eta$ -quenching is allowed.

### 2. SIMPLE MODEL

\*The National Center for Atmospheric Research is sponsored by the National Science Foundation  
Electronic address: gilman@hao.ucar.edu, rempel@hao.ucar.edu

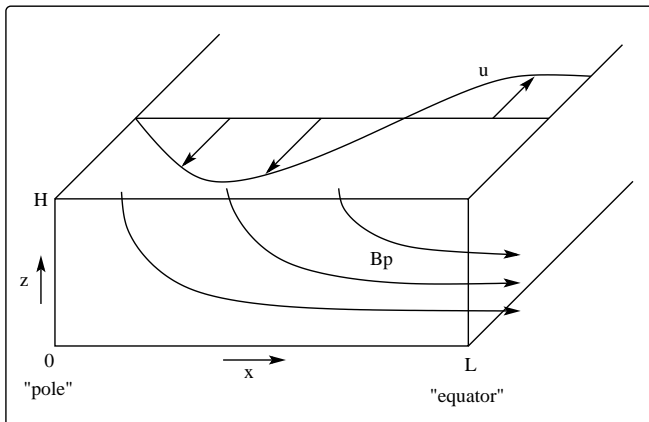


FIG. 1.— Schematic view of the geometry of our domain. Indicated are also the imposed velocity field  $u$  and the poloidal magnetic field  $B_p$ .

There are several levels of complexity that could be used to illustrate how  $\eta$ -quenching works. We choose here to work primarily in Cartesian geometry, since that allows us to obtain exact analytical solutions to illustrate the effect. We have also used a Cartesian finite difference code to compute the time dependent solutions of the induction equation and the reaction of the induced  $\mathbf{j} \times \mathbf{B}$  force on the differential rotation.

### 2.1. Governing Equations

For our model, we consider a channel that has an  $x-z$  cross section, infinite in the down channel coordinate. Sidewalls are at  $x = 0, L$ , bottom and top at  $z = 0, H$ . Roughly speaking, the  $x$  coordinate corresponds to colatitude on the Sun, the  $y$  coordinate, longitude and the  $z$  coordinate the vertical. The "pole" would be at  $x = 0$ , the "equator" at  $x = L$ . The geometry of the system is sketched in Figure 1.

For the form of  $\eta$ -quenching, we assume

$$\eta = \frac{\eta_0}{1 + (B/B_s)^2}, \quad (1)$$

in which  $\eta_0$  is the unquenched value,  $B = B(x, z)$  is the toroidal field to be solved for, and  $B_s$  is a constant, the value at which we assume  $\eta$  has been reduced by 50%.

We seek solutions for the toroidal field  $B(x, z, t)$ . The induction equation for this problem is given by

$$\begin{aligned} \frac{\partial B}{\partial t} = & B_x \frac{\partial u}{\partial x} + B_z \frac{\partial u}{\partial z} + \frac{\partial}{\partial x} \left( \frac{\eta_0}{1 + (B/B_s)^2} \frac{\partial B}{\partial x} \right) \\ & + \frac{\partial}{\partial z} \left( \frac{\eta_0}{1 + (B/B_s)^2} \frac{\partial B}{\partial z} \right), \end{aligned} \quad (2)$$

in which  $u$  is the assumed differential rotation, and  $B_x, B_z$  is the assumed poloidal field. We require

$$\frac{\partial B_x}{\partial x} + \frac{\partial B_z}{\partial z} = 0 \quad (3)$$

but allow  $B_x$  and/or  $B_z$  to cross the "equatorial" and/or top boundaries. For simplicity we omit meridional circulation from this calculation.

There is a key transformation of the diffusion terms in equation (2) that allows us to find analytical solutions, at

least in the case of an assumed steady state. In particular from Buringtons tables, page 38,

$$\frac{1}{1 + f^2} \frac{df}{dx} = \frac{d}{dx} \tan^{-1} f \quad (4)$$

from which we can write

$$\begin{aligned} \frac{\partial B}{\partial t} = & B_x \frac{\partial u}{\partial x} + B_z \frac{\partial u}{\partial z} \\ & + \eta_0 B_s \left( \frac{\partial^2}{\partial x^2} + \frac{\partial^2}{\partial z^2} \right) \tan^{-1} \left( \frac{B}{B_s} \right). \end{aligned} \quad (5)$$

As a starting point, we seek steady solutions to equation (5). If we define  $a = \tan^{-1}(B/B_s)$  then equation (5) reduces to

$$\left( \frac{\partial^2}{\partial x^2} + \frac{\partial^2}{\partial z^2} \right) a = -\frac{1}{\eta_0} \left( \frac{B_x}{B_s} \frac{\partial u}{\partial x} + \frac{B_z}{B_s} \frac{\partial u}{\partial z} \right), \quad (6)$$

a Poisson-type equation for specific  $B_x, B_z$  and  $u$ .

### 2.2. Assumptions for differential rotation an poloidal field

There are many choices for poloidal field and differential rotation. Trigonometric functions are particularly convenient and illustrative. We choose

$$\begin{aligned} u = & -U_0 \sin \left( \frac{3\pi x}{2L} \right) \sin \left( \frac{\pi z}{2H} \right), \\ B_x = & B_p \sin \left( \frac{\pi x}{2L} \right) \cos \left( \frac{\pi z}{2H} \right), \\ B_z = & -B_p \cos \left( \frac{\pi x}{2L} \right) \sin \left( \frac{\pi z}{2H} \right), \end{aligned} \quad (7)$$

in which  $U_0$  and  $B_p$  are constant. For these cases,  $u$  has a maximum at  $x = L$  (the "equator") and is zero at  $x = 2L/3$  ( $30^\circ$  "latitude") as well as at  $x = 0$  (the "pole"), very similar to the linear velocity of rotation on the Sun. There is also no differential rotation with  $x$  at the bottom, and a maximum amount at the top (analogous to the solar tachocline). The poloidal field  $B_z$  is a maximum at  $x = 0$ , and zero at  $x = L$ , corresponding to a dipole field crossing the equator.  $B_x$  is zero at  $x = 0$ , and a maximum at  $x = L$ . By substitution,  $B_x, B_z$  satisfy equation (3). All these fields are shown schematically in Figure 1. Obviously many other choices of poloidal field and differential rotation are possible, but these seem particularly relevant to the solar case.

### 2.3. Solution

Substitutions of equations (7) into the right-hand side of (6) yields

$$\begin{aligned} \left( \frac{\partial^2}{\partial x^2} + \frac{\partial^2}{\partial z^2} \right) a = & \frac{B_p}{B_s} \frac{\pi}{4L^2} R_m \sin \left( \frac{\pi z}{H} \right) \left[ 3 \sin \left( \frac{\pi x}{2L} \right) \right. \\ & \left. \cos \left( \frac{3\pi x}{2L} \right) - \cos \left( \frac{\pi x}{2L} \right) \sin \left( \frac{3\pi x}{2L} \right) \right] \end{aligned} \quad (8)$$

in which  $R_m = U_0 L / \eta_0$  is a magnetic Reynolds number. By inspection, equation (8) should yield separable solutions

$$a = g(x) \sin \left( \frac{\pi z}{H} \right), \quad (9)$$

from which we get

$$B = B_s \tan \left[ g(x) \sin \left( \frac{\pi z}{H} \right) \right]. \quad (10)$$

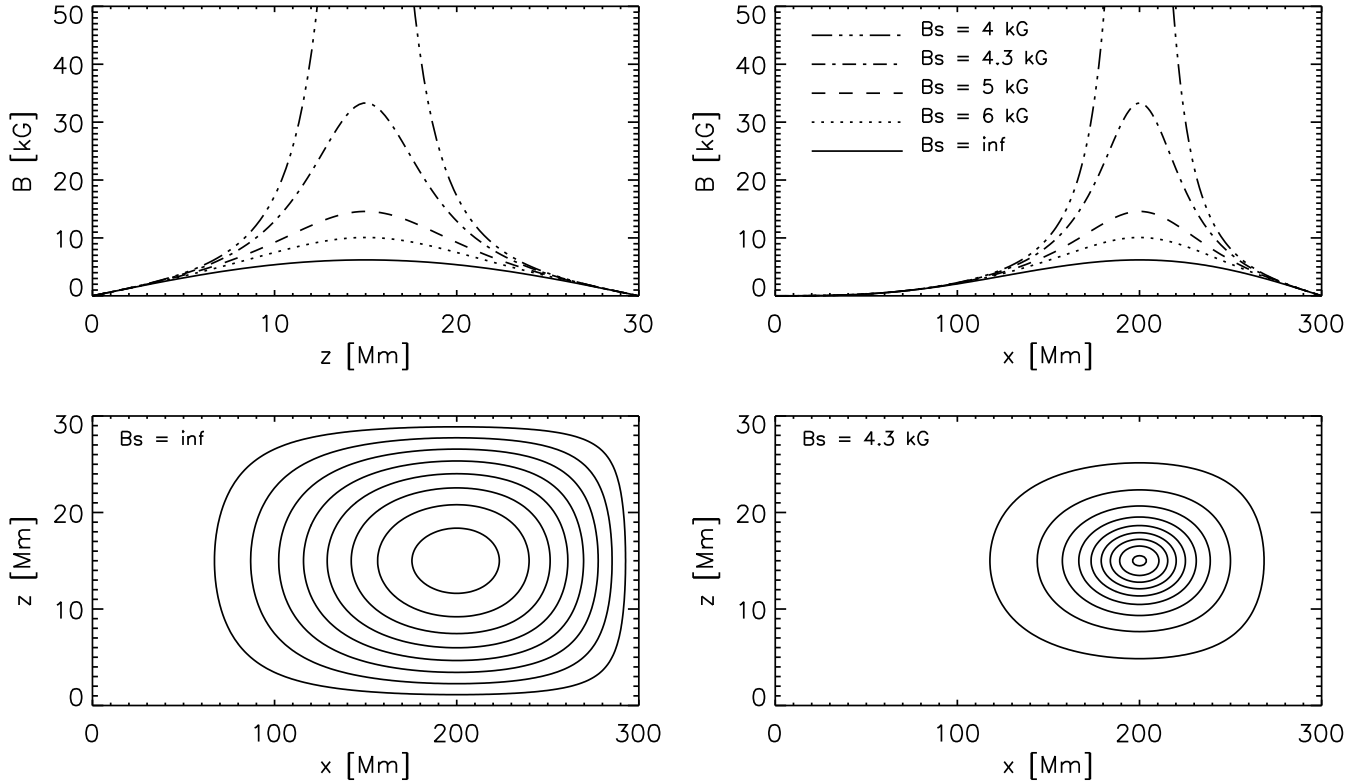


FIG. 2.— Solutions of equation (13). The top panels show a vertical cross section at  $x = 200$  Mm =  $2/3 L$  (left) and a horizontal cross section in the middle of the domain (right). The bottom panels show contours of the toroidal field for two distinct cases. Common parameters are  $R_m = 3000$ ,  $H/L = 0.1$ , and  $B_p = 1$  kG. Solutions are shown for  $B_s = \infty$ , 6, 5, 4.3, and 4 kG.

The tangent function is particularly critical in determining the form of the toroidal field  $B$ . The substitution of equation (9) into equation (8), and changing variables by letting  $x = 2L\lambda/\pi$  leads to

$$\frac{d^2 g}{d\lambda^2} - 4 \left( \frac{L}{H} \right)^2 g = \frac{B_p R_m}{B_s \pi} [3 \sin \lambda \cos 3\lambda - \cos \lambda \sin 3\lambda] \quad (11)$$

For the solar tachocline, we can argue that  $L/H \gg 1$  (typical values are around 10 – 30) to a first approximation, so we can ignore the second derivative term in equation (11) (unless we need to include a boundary layer to satisfy a boundary condition). In that case

$$g(x) = \frac{B_p}{B_s} \left( \frac{H}{L} \right)^2 \frac{R_m}{4\pi} \left[ \cos \left( \frac{\pi x}{2L} \right) \sin \left( \frac{3\pi x}{2L} \right) - 3 \sin \left( \frac{\pi x}{2L} \right) \cos \left( \frac{3\pi x}{2L} \right) \right] \quad (12)$$

and therefore the full solution for  $B$  is

$$B = B_s \tan \left\{ \frac{B_p}{B_s} \left( \frac{H}{L} \right)^2 \frac{R_m}{4\pi} \sin \left( \frac{\pi z}{H} \right) \left[ \cos \left( \frac{\pi x}{2L} \right) \sin \left( \frac{3\pi x}{2L} \right) - 3 \sin \left( \frac{\pi x}{2L} \right) \cos \left( \frac{3\pi x}{2L} \right) \right] \right\} \quad (13)$$

Thus we have found exact analytic solutions to a nonlinear partial differential equation!

#### 2.4. Qualitative Interpretation

The solution given in equation (13), a particular case of the more general solution given in equation (10), reveals many qualitative features, evident even without plotting. Of primary interest is that the induced toroidal field is proportional to the tangent of a function, of latitude and height, the magnetic Reynolds number, the ratio of assumed poloidal field to the quenching toroidal field, and the 'aspect ratio' of the domain, which is small in the actual solar tachocline. As is well-known, when the argument  $p$  of a tangent function is small, then  $\tan p \approx p$ . In this limit, equation (13) becomes independent of the  $\eta$ -quenching field  $B_s$ . But  $\tan p$  approaches infinity as the argument  $p$  approaches  $\pi/2$ . So we have the possibility of very large amplification of the toroidal field from an initially relatively small poloidal field, as well as compared to  $B_s$ .

From equation (13) the induced toroidal field always vanishes at the 'pole' at  $x = 0$ , as well as the 'equator' at  $x = L$ , and the top and the bottom of the layer. This is true even though the poloidal field crosses both the top boundary at  $z = H$  and the side boundary at  $x = L$ . Therefore the toroidal field is contained within the domain of induction, and peaks in amplitude at mid height,  $z = H/2$ . In addition, by inspection of equation (13), we can deduce that the argument of the tangent always has a peak at  $x = 2L/3$  the equivalent of  $30^\circ$  latitude on the Sun. Obviously this location is a function of our assumptions, but it follows from a differential rotation similar to

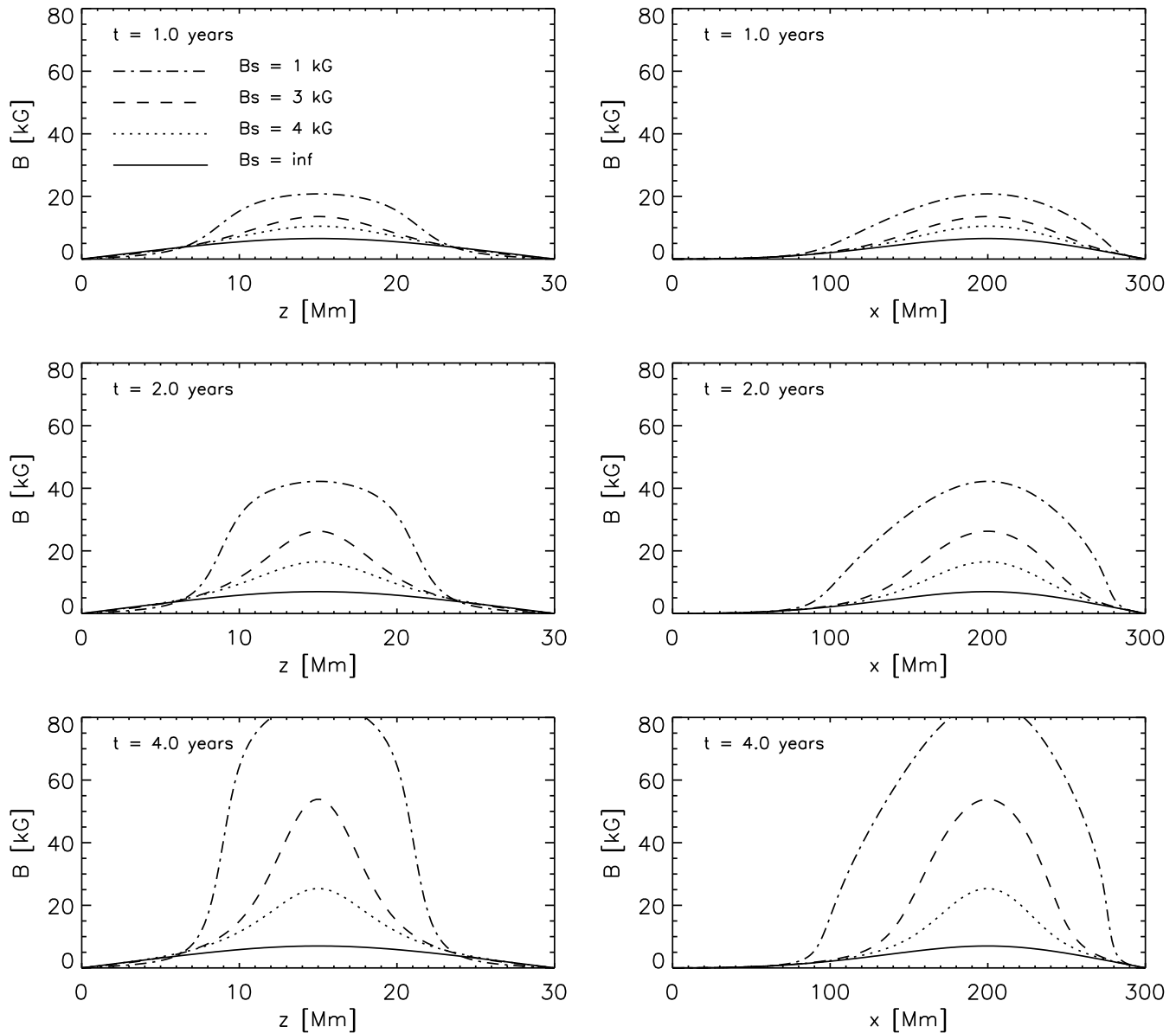


FIG. 3.— Snapshots of time dependent solution after 1, 2, and 4 years. Shown are vertical cross sections at  $x = 200 \text{ Mm} = 2/3 L$  (left panels) and horizontal cross sections (right panels) at  $z = 15 \text{ Mm} = 1/2 H$  of the toroidal field. Each panel shows a solution with no  $\eta$ -quenching (solid),  $\eta$ -quenching with  $B_s = 4 \text{ kG}$  (dotted),  $\eta$ -quenching with  $B_s = 3 \text{ kG}$  (dashed), and  $\eta$ -quenching with  $B_s = 1 \text{ kG}$  (dashed-dotted).

that of the Sun, and a 'dipole-like' poloidal field, so its location near the latitude where spots are first seen in a new sunspot cycle may not be coincidence.  $B_s$  is always positive, so for positive poloidal field  $B_p$ , the induced toroidal field is positive everywhere in the domain, even though not all terms in the induction forcing function (the right hand side) of equation (6) contribute with the same sign.

Given the above, then, we can expect larger amplification of the toroidal field in the interior of the domain, peaking at mid-depth and  $x = 2L/3$  or about  $30^\circ$  latitude. There can easily be a finite thickness and finite  $x$  or latitude range where the argument of the tan exceeds  $\pi/2$ . What does this mean? In the section 3, we discuss reaching the steady solutions represented by equa-

tion (13) via time-dependent simulations that start from a state with zero toroidal field. We argue here that such solutions on the 'other side' of  $\pi/2$  are not attainable in a finite time; the domain of such 'unreachable' solutions would be defined by the contour in the interior of our domain on which, for given  $B_p$ ,  $B_s$  and  $R_m$ , the argument of the tan  $= \pi/2$ . On this contour, in effect steady solutions do not exist, because they would take an infinite time to reach the infinite field value.

But so long as the argument of the tan remains smaller than  $\pi/2$  in the whole domain, steady solutions are well defined throughout. Even in this case, however, it is of interest to know as a function of various parameters how long it takes a time-dependent solution to 'spin up' to the steady state. Obviously solutions that take the order

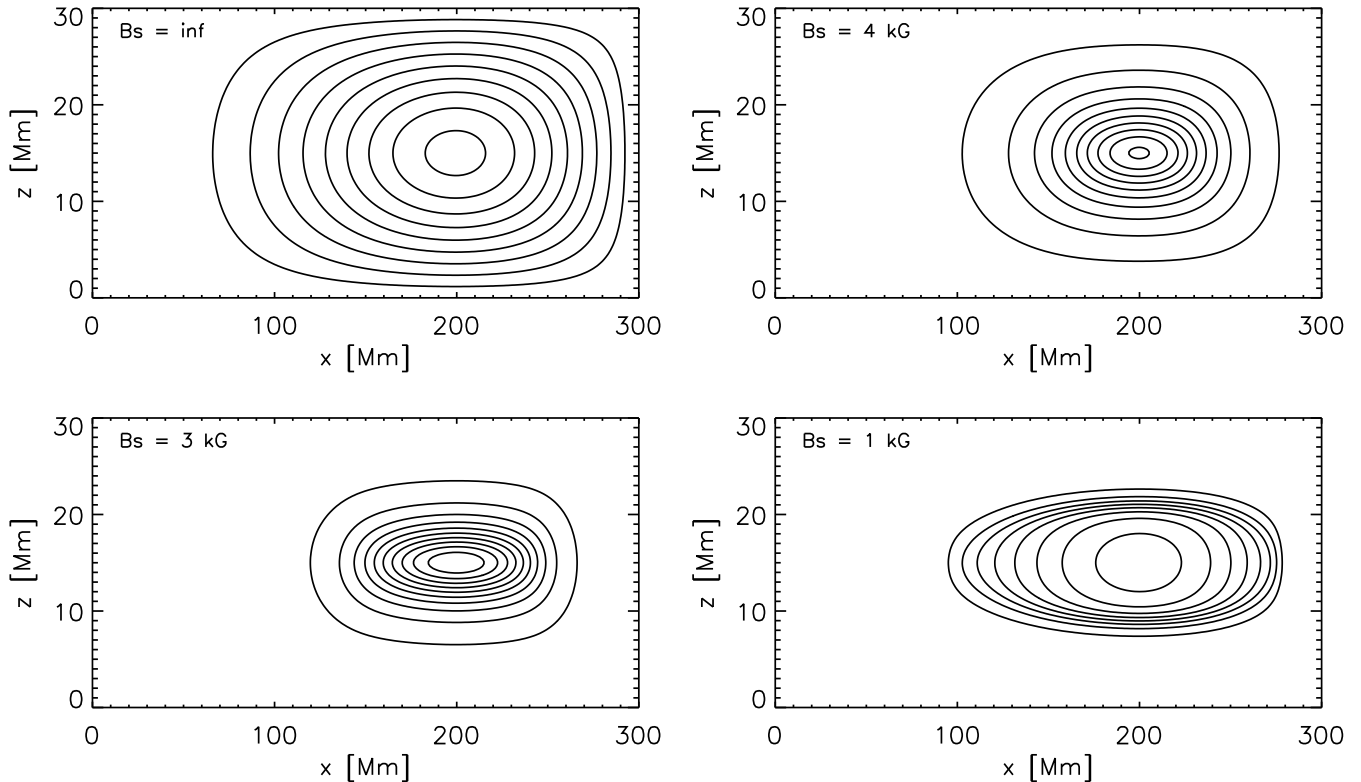


FIG. 4.— Contours of the toroidal field after 4 years of amplification for the different values of  $B_s$  used for Figure 3.  $\eta$ -quenching tends to concentrate field close to the peak value.

of a sunspot cycle or longer to reach the steady state will generally not be realized in the sun, since the cycle progresses and the peak toroidal field moves in latitude.

The differences in predicted toroidal field amplitude as functions of  $B_s$ ,  $B_p$ , and  $R_m$  in equation (13) are straightforward to understand. Since the larger is  $R_m$ , the lower is the unquenched diffusivity, so we should expect larger toroidal fields to result from a given  $B_p$ . And obviously the larger is  $B_p$  initially, the larger will be the resulting toroidal field. But the toroidal field is larger the smaller is  $B_s$ , since  $B_s$  is in the denominator inside the tangent function and in the numerator outside. This is because for smaller  $B_s$ , the local diffusivity is reduced starting at lower toroidal field, and so locally the toroidal field is kept from diffusing away; hence it amplifies further. For low enough  $B_s$ , so strong is the induction that no steady state can be reached.

### 2.5. Quantitative results

Figure 2 shows solutions of equation (13) for the common parameters  $R_m = 3000$ ,  $H/L = 0.1$ , and  $B_p = 1$  kG. To illustrate the amplification and concentration effect of  $\eta$ -quenching we have shown solutions for  $B_s = \infty$ , 6, 5, 4.3, and 4 kG. The top panels show a vertical cross section at  $x = 200$  Mm (left) and a horizontal cross section in the middle of the domain (right). The bottom panels show contours of the toroidal field for the cases with  $B_s = \infty$  (left) and  $B_s = 4.3$  kG. The case with  $B_s = 4$  kG shown in the top panels is close to the transition toward unbounded solutions (the peak field strength is around 200 kG). Figure 2 shows clearly the significant

amplification and concentration effect discussed qualitatively in section 2.4 before.

### 2.6. Solar effects?

For plausible values of all the parameters in equation (13), will the amplification effect we have found be significant for the Sun, in particular the solar tachocline? In the tachocline, we estimate that  $30 \text{ ms}^{-1} \leq U_0 \leq 100 \text{ ms}^{-1}$ ;  $10^9 \text{ cm}^2 \text{ s}^{-1} \leq \eta_0 \leq 10^{11} \text{ cm}^2 \text{ s}^{-1}$ , from weak overshooting turbulence there;  $3 \times 10^5 \text{ km} \leq L \leq 10^6 \text{ km}$ . These values lead to  $10^3 \leq R_m \leq 10^6$ . For a tachocline of thickness  $H \sim 3 \times 10^4 \text{ km}$ ,  $0.03 \leq H/L \leq 0.1$ . Plausible ranges for  $B_p$  and  $B_s$  are  $5 \times 10^2 \text{ G} \leq B_p \leq 5 \times 10^3 \text{ G}$  and  $10^3 \text{ G} \leq B_s \leq 10^4 \text{ G}$ . Then

$$4 \times 10^{-3} \leq \frac{1}{4\pi} \frac{B_p}{B_s} \left( \frac{H}{L} \right)^2 R_m \leq 4 \times 10^3 \quad (14)$$

so in the Sun there is a full range of amplification possible, from extremely small to extremely large, depending on the values of the various parameters we choose. Given that the peak value of the trig functions inside of equation (13) is about 2.6, with  $\pi/2 = 1.57$  corresponding to infinite amplification; mid-range values for all parameters in (14) leads to an argument of the tangent for the solar tachocline of  $\sim 10$ , a factor of 6 above the first infinity. Thus it is easy to have solar conditions for which the amplification is large.

## 3. TIME DEPENDENT SOLUTIONS

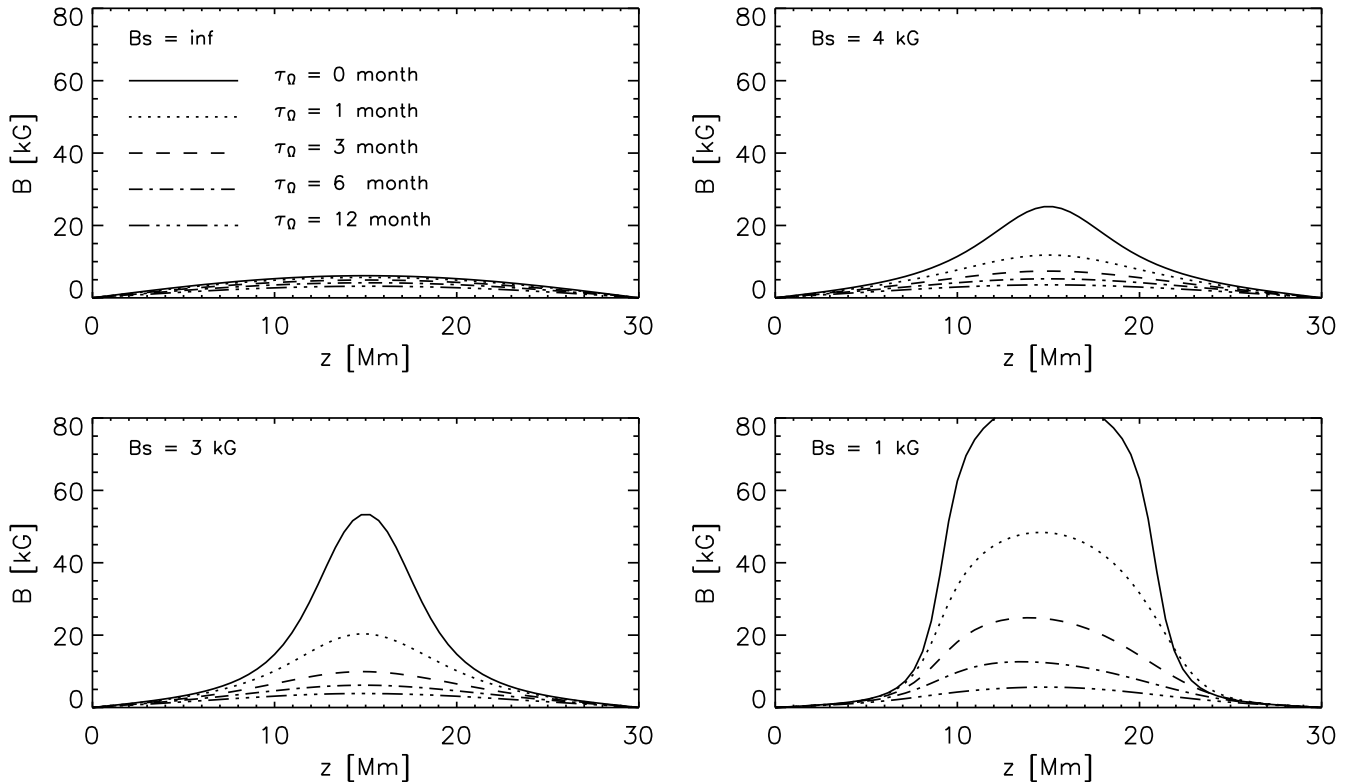


FIG. 5.— Influence of feedback on differential rotation on amplification process. We show snapshots of the solutions after 4 years. In each panel the solid line indicates the solutions presented already in Figure 3, the dotted, dashed, dashed-dotted, and triple-dashed-dotted lines represent solutions including feedback through Lorentz force and a restoration time scale for the differential rotation of  $\tau = 1, 3, 6, 12$  months, respectively.

There are at least two effects not included in the solutions in (13) that could significantly diminish the amplification effect on time scales relevant to a sunspot cycle. One, that we have already mentioned, is that the steady state is not reached before the solar cycle toroidal field moves to a lower latitude. The second is that as the toroidal field grows, there should develop a  $\mathbf{j} \times \mathbf{B}$  reaction force which damps the differential rotation responsible for the induction. Here we explore both of these effects with time dependent numerical calculations.

We first focus on time dependent solutions only solving the induction equation and neglecting the feedback of the magnetic field on the shear flow. To this end we solve equation (5) using a finite difference code. We tested our numerical setup by comparing the stationary solution obtained through our code with the solution shown in equation (13). For this comparison we have chosen the parameters in our numerical setup such that the argument of the tangent in equation (13) does not exceed  $\pi/2$  anywhere in the domain to ensure the existence of a stationary solution.

Common parameters for the time dependent solutions discussed below are:  $L = 3 \times 10^5$  km,  $H = 3 \times 10^4$  km,  $\eta_0 = 10^{11}$  cm<sup>2</sup> s<sup>-1</sup>,  $U_0 = 100$  ms<sup>-1</sup>, and  $B_p = 1$  kG. With this choice of parameters we have  $R_m = 3000$ ,  $H/L = 0.1$  and from equation (13) it can be expected that the argument of the tangent exceeds  $\pi/2$  if  $B_s = 4$  kG. Figure 3 shows snapshots of time dependent solutions after 1 year, 2 years, and 4 years. The panels

on the left show vertical cross sections at  $x = 200$  Mm, where the field peaks in the horizontal coordinate. The panels on the right show horizontal cross sections in the middle of the domain ( $z = 15$  Mm). We show a solutions with no  $\eta$ -quenching (solid line) and solutions with a value of  $B_s$  of 4 kG (dotted), 3 kG (dashed), and 1 kG (dashed-dotted). We can achieve similar toroidal field amplification patterns with  $B_s$  set much higher simply by assuming a smaller  $\eta_0$  and therefore a larger  $R_m$ . As explained above the solution with  $B_s = 4$  kG marks the transition from asymptotically stationary to unbounded solutions. The solution with no  $\eta$ -quenching reaches an asymptotic field strength of around 6 kG, whereas the solution with  $B_s = 1$  kG reaches around 80 kG after 4 years of amplification through the shear flow. Even the solution with moderate quenching  $B_s = 4$  kG reaches after 4 years a value more than three times larger than the reference solution with no  $\eta$ -quenching. Therefore it can be expected that the influence of  $\eta$ -quenching becomes visible even on time scales of the solar cycle.

As an additional effect, the  $\eta$ -quenching leads to a confinement of the magnetic field around the peak value, leading to a magnetic layer of less extent in radius and latitude compared to the reference solution with no quenching. The effect of confinement is largest for values of  $B_s$  close to the critical value for which only the most central part of the magnetic field gets significantly amplified ( $B_s = 3$  kG and 4 kG), whereas strong quenching ( $B_s = 1$  kG) leads to a significant amplification of a

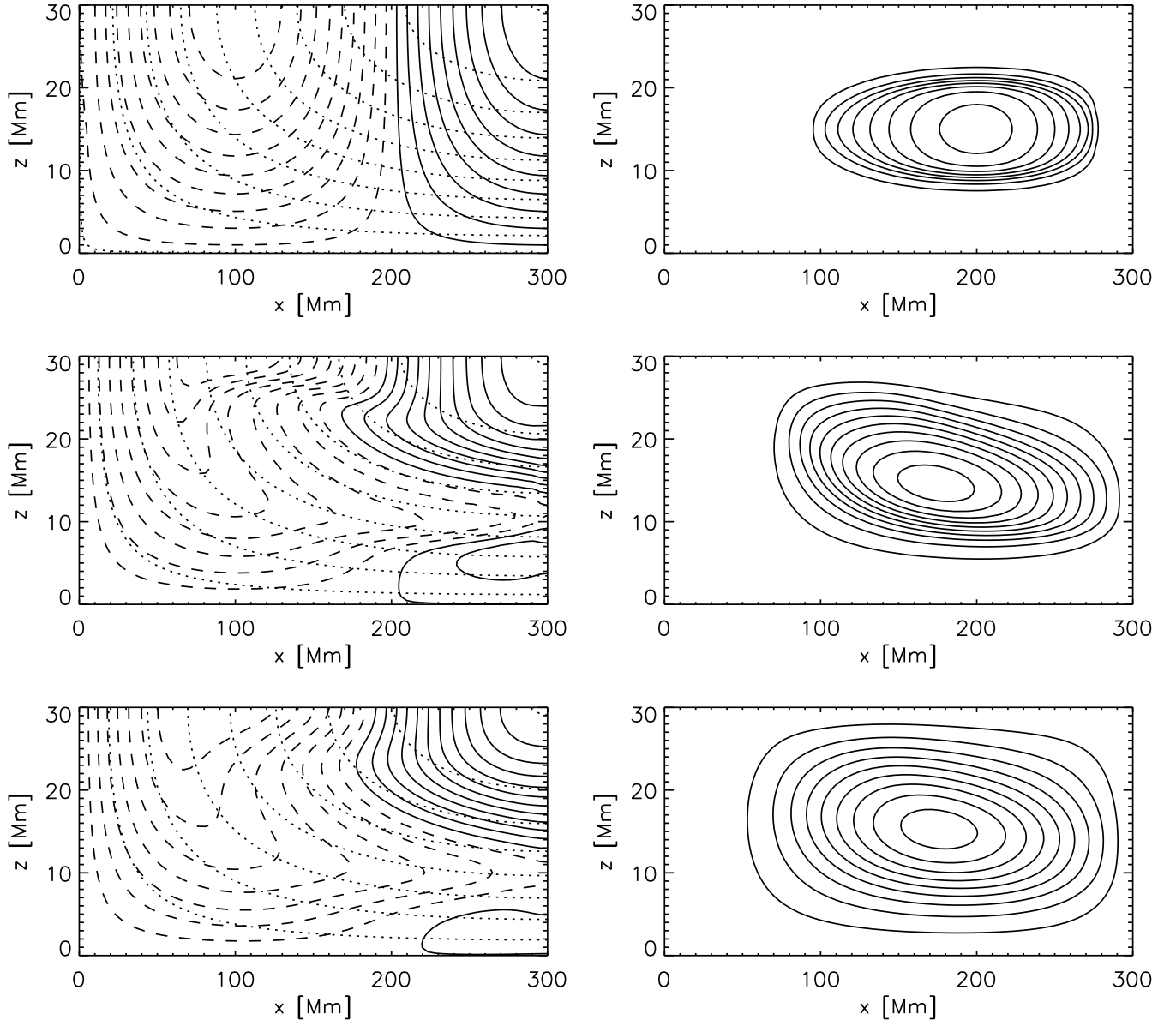


FIG. 6.— Contours of differential rotation (left panels) and toroidal field (right panels). The dotted curves in the left panels are the poloidal field lines. The top panels show the reference solution with no feedback, the middle panels the solution with  $\tau = 3$  months, and the bottom panels the solution with  $\tau = 12$  months. All snapshots are after 4 years of amplification time.

much broader field profile.

Figure 4 shows contour plots of the toroidal field after 4 years for the cases shown in Figure 3. The spacing of the contours is equidistant, ranging from 0 to the maximum value of each particular case. The greater concentration of toroidal flux around the center of the layer is clearly evident for  $B_s = 3$  and 4 kG.

The time dependent solutions discussed so far show clearly that a significant amplification of a 1 kG poloidal field to several tens of kG toroidal field can be achieved within a few years, if  $\eta$ -quenching is taken into consideration. However, these solutions assume that the feedback on the differential rotation through the Lorentz force can be neglected. In order to address this feedback in time dependent simulations we solve together with the induction equation an equation for the differential rotation of

the form

$$\frac{\partial u}{\partial t} = -\frac{u - u_0}{\tau} + \frac{1}{4\pi\varrho} \left( B_x \frac{\partial B}{\partial x} + B_z \frac{\partial B}{\partial z} \right) \quad (15)$$

In equation (15) we include a drag-type forcing term which replenishes the differential rotation from the convection zone above on a time scale  $\tau$ .  $u_0$  is the differential rotation in the case of no Lorentz force feedback. For the density  $\varrho$  we use a value of  $210 \text{ kg m}^{-3}$  to represent the overshoot region. Since there are currently no theories for the differential rotation in the tachocline, which would help to determine a reasonable value for  $\tau$ , we treat  $\tau$  as a free parameter and study the dependence of the solution on particular choices of values in the range of 1 month to 1 year. Differential rotation models for the entire convection zone (Miesch et al. 2000; Brun & Toomre

2002; Rempel 2005) typically predict a time scale of several years; however, this time scale should be shorter if only the tachocline is considered.

Figure 5 shows the influence of the feedback on differential rotation for different values of  $\tau$  ranging from 1 month to 1 year. In each panel is shown the vertical profile of the toroidal field at  $x = 200$  Mm; the solid line corresponds to the solutions shown in Figure 3 after 4 years. Even if a very short time scale for  $\tau$  of 1 month is used, the peak field strength reached is reduced by a factor of 2 in the cases with quenching of  $\eta$  (the case with no  $\eta$ -quenching shows a much weaker dependence on  $\tau$  since the field strength is very weak anyway for this choice of parameters). For the choice of  $\tau = 1$  year the peak field strength barely exceeds 5 kG. However, the tendency that  $\eta$ -quenching leads to stronger and more confined field is still visible in all cases shown.

Figure 6 shows the profile of differential rotation (left panels) and toroidal magnetic field (right panels) for the cases with  $B_s = 1$  kG. The top panels show the reference solution with no feedback, the middle panels the solution with  $\tau = 3$  month and the bottom panels the solution with  $\tau = 1$  year. In the left panels solid lines indicate positive values of  $u$ , dashed lines negative values. We overplotted the field lines of the poloidal field to show how the contours of the velocity field get aligned with the poloidal field lines to minimize the induction effect (Ferraro's law of iso-rotation). As a consequence, the feedback through the Lorentz force moves the shear layer of the differential rotation upward close to the equator ( $x = 300$  Mm) and downward close to the pole ( $x = 0$  Mm), leading to a significant reduction of the latitudinal shear in the middle of the domain, where the toroidal field peaks.

To summarize,  $\eta$ -quenching has a significant influence on the field amplification, even if the time available for amplification is limited to a few years to reflect the solar cycle variability. Including the feedback on differential rotation through Lorentz force leads to a significant decrease in the peak field strength reached; however, the influence of  $\eta$ -quenching remains visible in most cases. Unless time scales of less than 1 month for the replenishment of differential in the tachocline are assumed it seems impossible to amplify a magnetic field to 100 kG as inferred by simulations of rising flux tubes. Other amplification mechanisms that do not rely on differential rotation as energy source, as for example the explosion of magnetic flux tubes (Rempel & Schüssler 2001) or the downward draining of their interiors, most probably also play an important role.

#### 4. CONCLUSIONS AND DISCUSSION

We have demonstrated with a simple Cartesian model that the damping of turbulent magnetic diffusivity by the growth of strong toroidal fields is a powerful mechanism for making such fields even stronger and more concentrated. Even though the expected reaction of these stronger fields on the differential rotation that induced them can limit the amplitude of this effect, it should remain an important contributor to the overall operation of the dynamo inside the Sun.

Our result is qualitatively consistent with the effect common to all flux transport and interface dynamos for the sun, in which the high toroidal field in the tachocline is achieved because of the low magnetic diffusivity there. In that case, the low diffusivity comes from the assumed weak turbulence there, while in the present work the toroidal field is assumed to locally reduce the turbulence. This quenching has already been shown by Tobias (1996) to have profound effects on, for example, dynamo mode type, when applied to more idealized interface dynamos considered for the bottom of the convection zone.

The role this toroidal field amplification mechanism plays in current dynamo models for the Sun should be tested. While our model used Cartesian geometry because of its simplicity and because it yielded useful analytical solutions, we have done sample calculations in spherical geometry that show similar effects will be present there.

It will be interesting to see even in the kinematic dynamo regime how much concentration and amplification of toroidal field occurs when a real dynamo solution is advancing through a simulated solar cycle, so the toroidal field is continually moving toward the equator. This effect could also be simulated with our simple Cartesian model by taking poloidal fields that represent various phases of a solar cycle; the case we have chosen corresponds roughly to the maximum phase, since the poloidal field peaks at the pole and there are no separate 'old' and 'new' cycle poloidal fields present. It is clear from our basic equations that analytic solutions should also exist for these other cycle phases. An important factor limiting toroidal field amplification will be simply how long in reality it takes for the imposed poloidal field to move in  $x$  (latitude) enough to change significantly the location where induction of toroidal field is strongest.

The authors thank Mausumi Dikpati for helpful comments on a draft of this paper. We also thank the anonymous referee for a very helpful review.

#### REFERENCES

- Brun, A. S. & Toomre, J. 2002, *ApJ*, 570, 865  
 Caligari, P., Moreno-Insertis, F., & Schüssler, M. 1995, *ApJ*, 441, 886  
 Caligari, P., Schüssler, M., & Moreno-Insertis, F. 1998, *ApJ*, 502, 481  
 Choudhuri, A. R. & Gilman, P. A. 1987, *ApJ*, 316, 788  
 Dikpati, M. & Charbonneau, P. 1999, *ApJ*, 518, 508  
 Fan, Y., Fisher, G. H., & McClymont, A. N. 1994, *ApJ*, 436, 907  
 Miesch, M. S., Elliott, J. R., Toomre, J., Clune, T. L., Glatzmaier, G. A., & Gilman, P. A. 2000, *ApJ*, 532, 593  
 Moreno-Insertis, F., Caligari, P., & Schüssler, M. 1995, *ApJ*, 452, 894  
 Rüdiger, G. & Kitchatinov, L. L. 2000, *Astronomische Nachrichten*, 321, 75  
 Rüdiger, G., Kitchatinov, L. L., Küker, M., & Schultz, M. 1994, *Geophysical and Astrophysical Fluid Dynamics*, 78, 247  
 Rempel, M. 2005, *ApJ*, 622, 1320  
 Rempel, M. & Schüssler, M. 2001, *ApJ*, 552, L171  
 Schüssler, M., Caligari, P., Ferriz-Mas, A., & Moreno-Insertis, F. 1994, *A&A*, 281, L69  
 Tobias, S. M. 1996, *ApJ*, 467, 870  
 Vainshtein, S. I. & Cattaneo, F. 1992, *ApJ*, 393, 165